

Characterization of $\text{Li}_{1-x}\text{Ni}_{1+x}\text{O}_2$ Prepared Using Succinic Acid as a Complexing Agent¹

Titipun Thongtem and Somchai Thongtem

Faculty of Science, Chiang Mai University, Chiang Mai, 50200 Thailand

e-mail: tpthongtem@yahoo.com; tpthongtem@hotmail.com

Received March 25, 2005; in final form, September 22, 2005

Abstract— $\text{Li}_{1-x}\text{Ni}_{1+x}\text{O}_2$ was prepared by a polymerized complex method using succinic acid as a complexing agent. Ethanolic solutions of lithium acetate dihydrate, nickel acetate tetrahydrate, and succinic acid were mixed to form carboxylate precursors, which were subsequently calcined at 650–800°C for 14–48 h. TGA curves of metal acetates, succinic acid, and the precursors were characterized to determine weight loss and formation temperature of the oxide. By using XRD, SEM, and EDX, pure crystals of $\text{Li}_{1-x}\text{Ni}_{1+x}\text{O}_2$ were detected at 750 and 800°C. The maximum and minimum intensity ratios of XRD spectra show that the optimum calcination condition is 750°C for 40 h. At 650–800°C, the particle size distribution is in the range of 0.35–39 μm.

DOI: 10.1134/S0020168506020166

INTRODUCTION

At present, the demand for rechargeable batteries in electronic devices becomes increasingly important. LiNiO_2 is an oxide of great interest due to its large discharge capacity [1], long cycle life [2], and low cost [2, 3]. It has a layered, $\alpha\text{-NaFeO}_2$ type structure with the rhombohedral space group $R\bar{3}m$ [4–6]. The preparation of the oxide with good electrochemical properties is rather difficult due to the formation of nonstoichiometric phase at high temperature [6–8]. Solid-state reaction, a physical process, can be done by heating a mixture at high temperature, but it is time-consuming [9, 10]. The reaction results in a nonstoichiometric phase [2, 7], inhomogeneity [7, 11], irregular morphology [7], and larger particle size and size distribution [7]. Therefore, low-temperature methods, such as the Pechini process [12], sol–gel method [13], precipitation process [14], and hydrothermal technique [11, 15], have been developed.

For the present research, $\text{Li}_{1-x}\text{Ni}_{1+x}\text{O}_2$ powder has been prepared by a polymerized complex method using succinic acid as a complexing agent with subsequent calcination at high temperature for certain time periods. Optimum conditions, phase, morphology, and size distribution have been evaluated.

EXPERIMENTAL

Following a similar preparation procedure for LiMn_2O_4 [16], $\text{Li}_{1-x}\text{Ni}_{1+x}\text{O}_2$ powder was prepared from two starting reagents (lithium acetate dihydrate and nickel acetate tetrahydrate) and a complexing agent

(succinic acid). Stoichiometric amounts of lithium and nickel salts and succinic acid were dissolved separately in ethanol, mixed, and subsequently heated at 50–60°C to remove ethanol. The carboxylate precursors were precalcined at 450°C to remove organic compounds and subsequently calcined at 650–800°C in air for 14–48 h. The preparation process is shown schematically in Fig. 1.

The carboxylate precursors and powder were characterized by a thermogravimetric analyzer (TGA) with

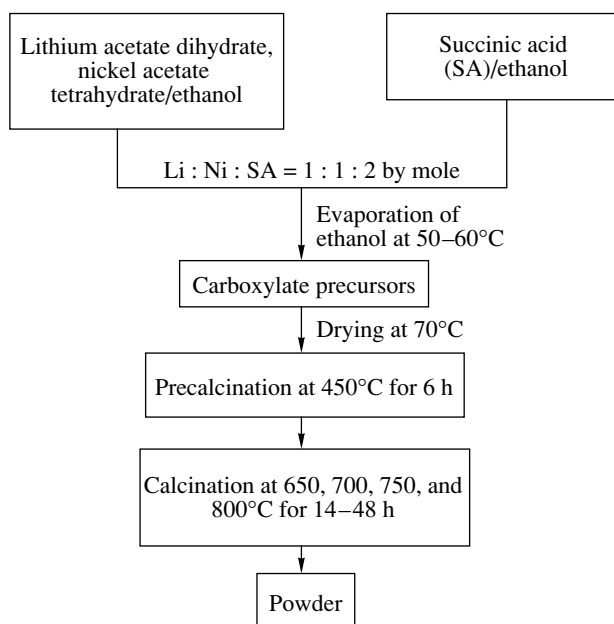


Fig. 1. Schematic diagram for the preparation of $\text{Li}_{1-x}\text{Ni}_{1+x}\text{O}_2$.

¹ The text was submitted by the authors in English.

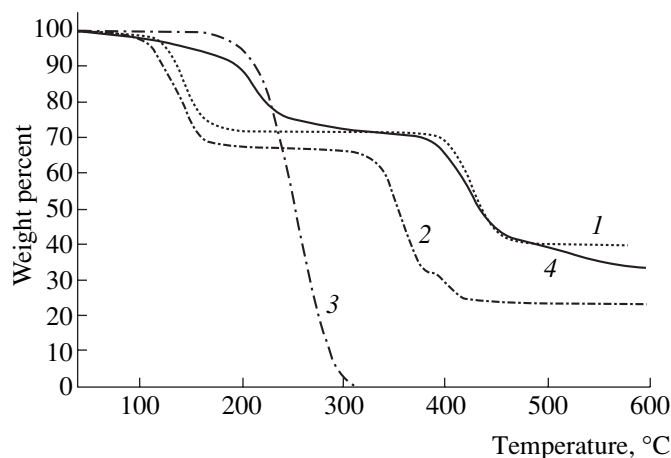


Fig. 2. TGA of (1) lithium acetate dihydrate, (2) nickel acetate tetrahydrate, (3) succinic acid, and (4) carboxylate precursors.

a heating rate of $20^\circ\text{C}/\text{min}$ in nitrogen atmosphere, an x-ray diffractometer (XRD) operated at 20 kV and 15 mA, using the K_α line from a Cu target, a scanning electron microscope (SEM) equipped with an energy dispersive x-ray (EDX) analyzer operated at 15 kV, a particle size analyzer (laser diffraction), an atomic

absorption spectrophotometer (AAS) to determine Li and Ni contents, and titration to determine Ni^{3+} ions. Ni^{3+} was reduced to Ni^{2+} by excess ammonium iron(II) sulfate and titrated back with a standard potassium permanganate solution.

RESULTS AND DISCUSSION

TGA. Lithium acetate dihydrate, nickel acetate tetrahydrate, succinic acid, and the carboxylate precursors were studied by TGA with the results shown in Fig. 2. The weight loss of lithium acetate dihydrate at $40\text{--}228$ and $338\text{--}470^\circ\text{C}$ is due to the evaporation of adsorbed water and water of crystallization (lattice water) and decomposition of acetate ions [17], respectively. Nickel acetate tetrahydrate shows a weight loss in three steps: evaporation of adsorbed and lattice water and decomposition of acetate ions and the residual organic constituents at $40\text{--}209$ [17], $271\text{--}390$ [17], and $390\text{--}500^\circ\text{C}$, respectively. Succinic acid shows a weight loss over the range of $170\text{--}320^\circ\text{C}$. Carboxylate precursors show a weight loss in four steps resulting from the evaporation of ethanol and adsorbed water at $40\text{--}170^\circ\text{C}$ and the decomposition of succinic acid, acetate ions from the pyrolysis of lithium and nickel acetates, and other organic compounds at $170\text{--}320$, $320\text{--}470$, and 470--

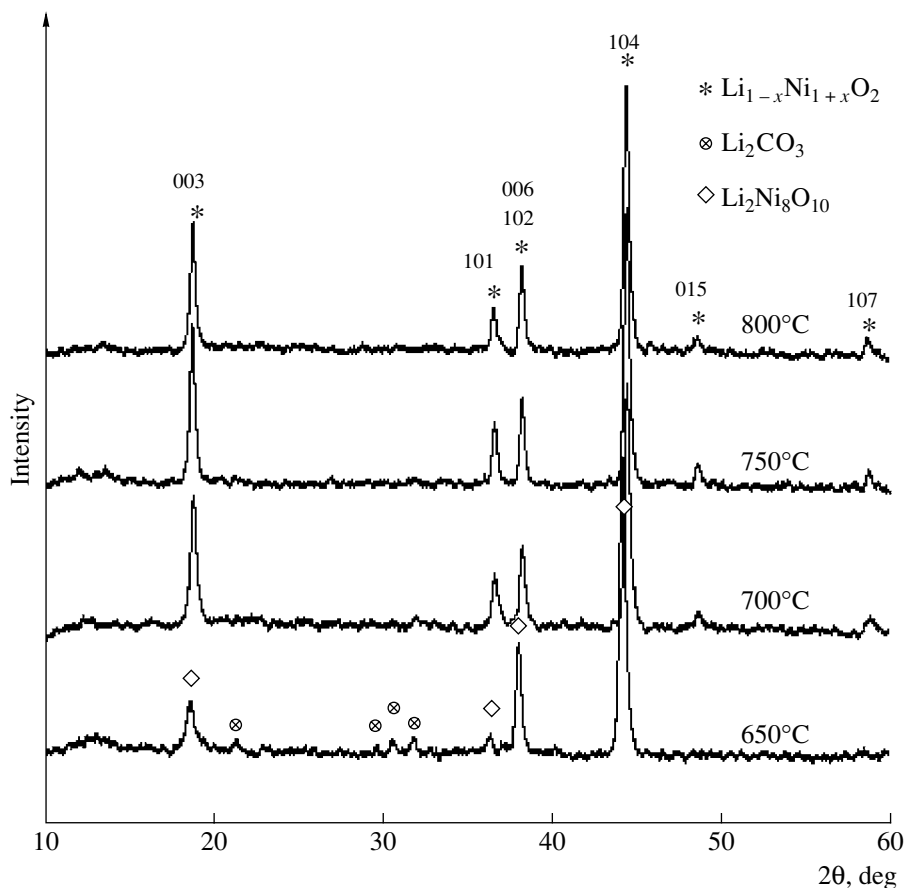


Fig. 3. XRD spectra of the powder produced at $650\text{--}800^\circ\text{C}$ calcination for 24 h.

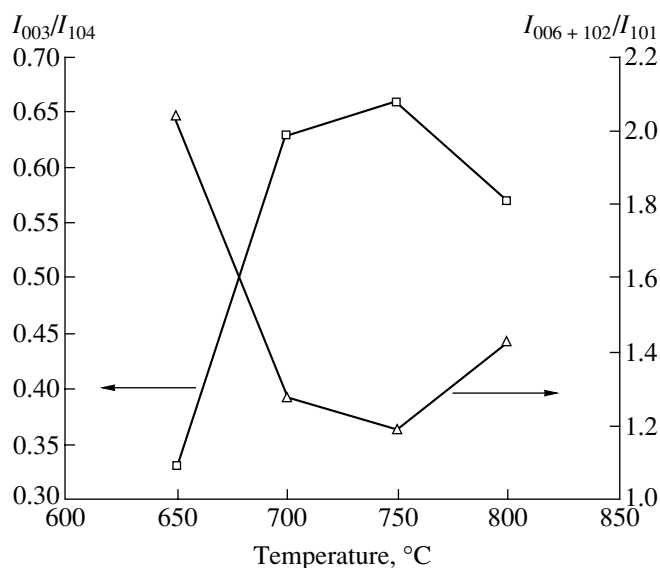


Fig. 4. I_{003}/I_{104} and $I_{006+102}/I_{101}$ intensity ratios at 650–800°C calcination for 24 h.

600°C, respectively. Succinic acid seems to influence the decomposition of acetate ions. After the weight loss is terminated, the formation of lithium nickel oxide is likely to begin at 600°C and higher temperatures.

XRD. The powder was analyzed using XRD and a JCPDS standard [18]. XRD spectra are shown in Fig. 3. At 650 and 700°C, the powder consists of $\text{Li}_{1-x}\text{Ni}_{1+x}\text{O}_2$ containing Li_2CO_3 and $\text{Li}_2\text{Ni}_8\text{O}_{10}$ impurities. At 750 and 800°C, the spectra were very sharp, and only the crystalline phase of $\text{Li}_{1-x}\text{Ni}_{1+x}\text{O}_2$ was detected. The diffraction angles of the experimental spectra are in accord with those of the standard, but the intensity I is slightly different. The I_{003}/I_{104} and $I_{006+102}/I_{101}$ intensity ratios at 650–800°C were calculated and plotted in Fig. 4. It was found that the intensity ratios were controlled by the evaporation of Li, which influences the oxide stoichiometry [12]. The I_{003}/I_{104} ratio increases with an increase in the calcination temperature to the maximum value at 750°C and decreases with further increase in temperature. Li and Ni ions are best ordered

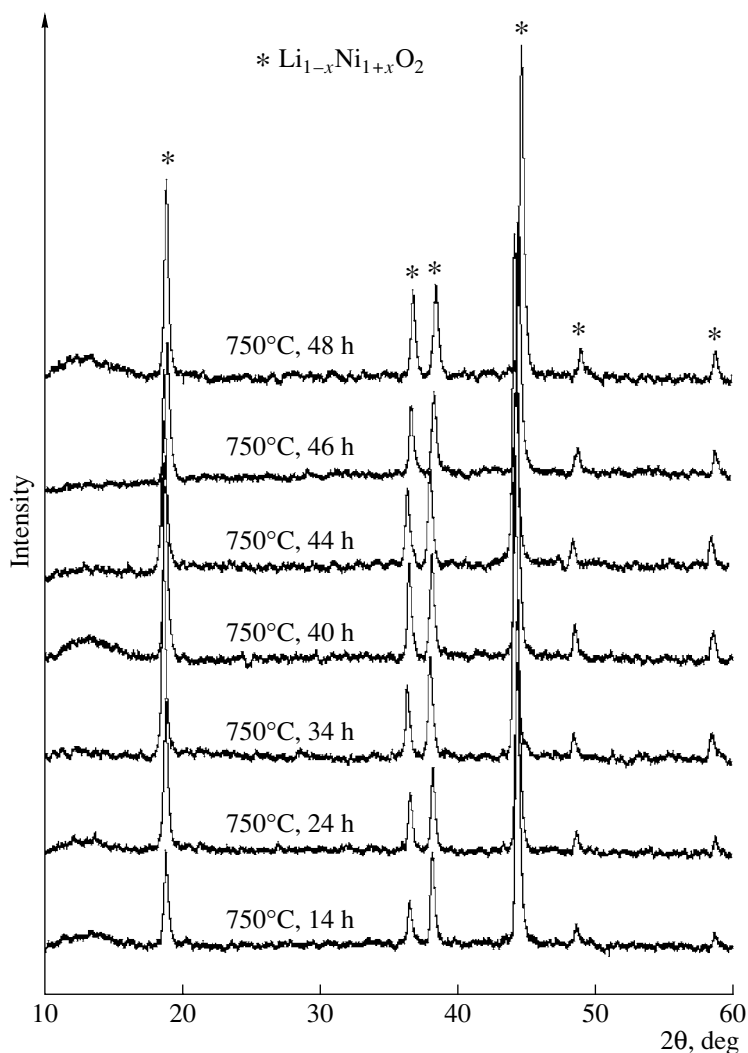


Fig. 5. XRD spectra of the powder produced at 750°C calcination for 14–48 h.

at 750°C [5, 7]. The $I_{006+102}/I_{101}$ ratio or R -factor is at a minimum at 750°C. The minimum intensity ratio is the parameter used to identify the best hexagonal ordering [5, 7, 19]. Due to the experimental results, the best hexagonal ordering or the best ordering of Li and Ni ions in $\text{Li}_{1-x}\text{Ni}_{1+x}\text{O}_2$ is at 750°C.

In order to find the optimum time for the preparation of $\text{Li}_{1-x}\text{Ni}_{1+x}\text{O}_2$, the calcination temperature was fixed at 750°C, and the experimental time was varied between 14 and 48 h. The XRD spectra are shown in Fig. 5. A single phase of $\text{Li}_{1-x}\text{Ni}_{1+x}\text{O}_2$ produced at 750°C for 14–48 h was detected. The spectra are very sharp, showing that the powder is crystalline. The I_{003}/I_{104} and $I_{006+102}/I_{101}$ intensity ratios for 14–48 h were calculated and are shown in Fig. 6. As the calcination time increases from 14 to 48 h, the I_{003}/I_{104} ratio increases to the maximum value at 40 h. The $I_{006+102}/I_{101}$ ratio is at a minimum at 40 h. The maximum and minimum intensity ratios are in accord. This reflects the best hexagonal ordering or cation ordering [5, 7, 19], which leads to the best electrochemical properties [7, 19].

Mean oxidation state of Ni. Li and Ni contents of the powder produced at 650–800°C calcination for 24 h were determined and are shown in Fig. 7. During calcination, the percent of Li decreases with increasing temperature due to the evaporation process. This leads to an increase of the percent of Ni. The mole ratios of Li and Ni at different temperatures were calculated, and the chemical formulas of lithium nickel oxide are shown in Table 1. The evaporation process reflects the stoichiometry of $\text{Li}_{1-x}\text{Ni}_{1+x}\text{O}_2$ and the oxidation state of Ni. The mean oxidation state of Ni was calculated using the equation

$$\text{Mean oxidation state of Ni} = 2 + N,$$

where N is the mole fraction of Ni^{3+} in the total mole of Ni. The $\text{Ni}^{3+}/(\text{Ni}^{3+} + \text{Ni}^{2+})$ ratio and mean oxidation state of Ni at different temperatures are also shown in Table 1. As the calcination temperature increases, the $\text{Ni}^{3+}/(\text{Ni}^{3+} + \text{Ni}^{2+})$ ratio and the mean oxidation state of Ni increase to the maximum value at the same temperature of 750°C and then decrease. In addition, the chemical formula, $\text{Ni}^{3+}/(\text{Ni}^{3+} + \text{Ni}^{2+})$, and the mean ox-

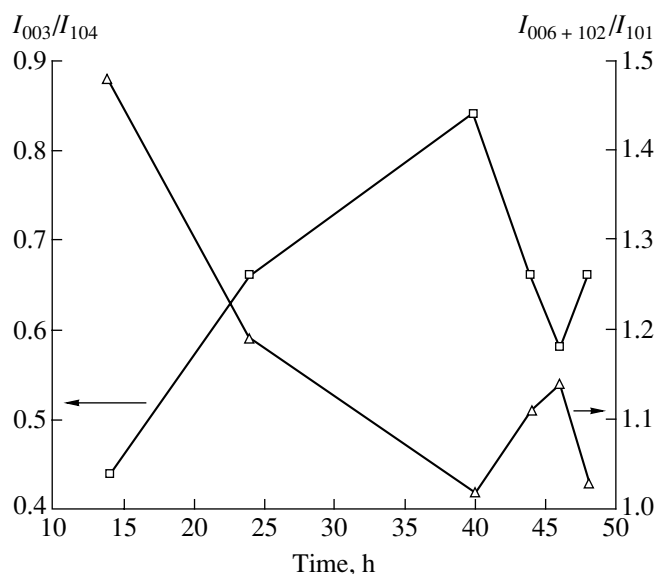


Fig. 6. I_{003}/I_{104} and $I_{006+102}/I_{101}$ intensity ratios at 750°C calcination for 14–48 h.

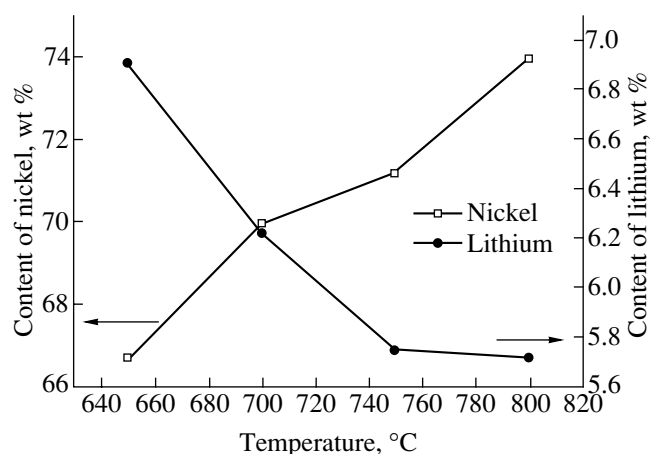


Fig. 7. Li and Ni contents of the powder produced at 650–800°C calcination for 24 h.

idation state of Ni at the best calcination condition (750°C, 40 h) were determined and are shown in Table 1.

Table 1. Chemical formulas, $\text{Ni}^{3+}/(\text{Ni}^{3+} + \text{Ni}^{2+})$ ratios, and mean oxidation states of Ni

Calcination conditions	Chemical formulas	$\text{Ni}^{3+}/(\text{Ni}^{3+} + \text{Ni}^{2+})$, wt %	Mean oxidation states of Ni
650°C, 24 h	$\text{Li}_{1.00}\text{Ni}_{1.14}\text{O}_2$	12.96	2.13
700°C, 24 h	$\text{Li}_{0.90}\text{Ni}_{1.19}\text{O}_2$	48.59	2.49
750°C, 24 h	$\text{Li}_{0.83}\text{Ni}_{1.21}\text{O}_2$	51.63	2.52
800°C, 24 h	$\text{Li}_{0.82}\text{Ni}_{1.26}\text{O}_2$	44.09	2.44
750°C, 40 h	$\text{Li}_{0.83}\text{Ni}_{1.22}\text{O}_2$	60.59	2.61

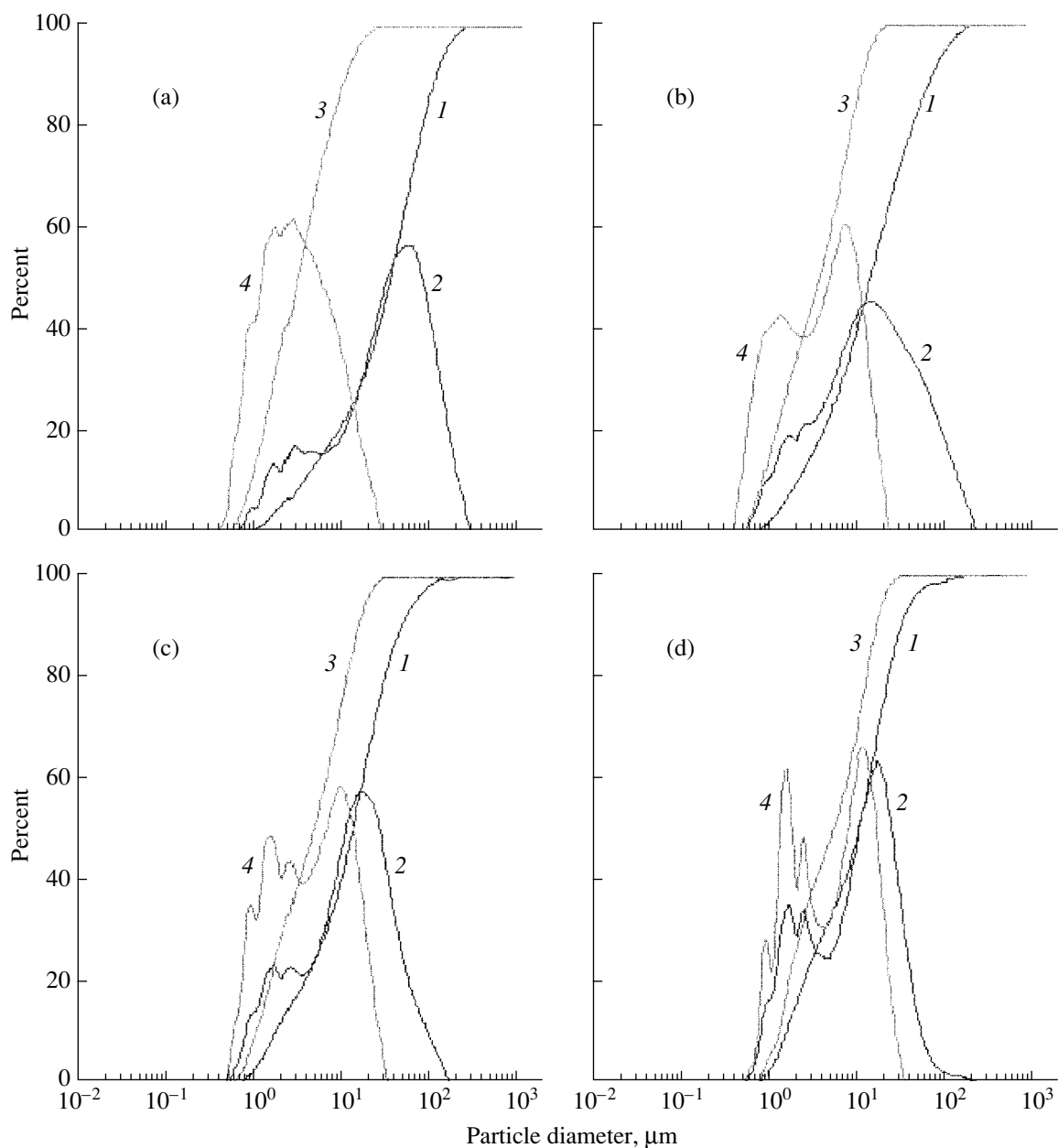


Fig. 8. Frequency and cumulative frequency distributions of the powder produced at (a) 650, (b) 700, (c) 750, and (d) 800°C calcination for 24 h: (1, 2) nonultrasonic vibration, (3, 4) ultrasonic vibration for 2 min.

Particle size distribution. Size distributions of the powder were determined using a particle size analyzer and are shown in Fig. 8. At 650–800°C calcination for 24 h, size distributions of the powder for nonultrasonic and ultrasonic vibrations are not normal and are over the range of 0.5–272 and 0.35–39 μm , respectively. This shows that ultrasonic vibration may influence the range of size distribution. The cumulative frequency distribution shows that the particles started to count and arrange from the smallest value. The volume diameter of 10, 50, and 90% powder (D_{10} , D_{50} , and D_{90}) and volume mean diameter (mean) were determined and are shown in Table 2. In case of nonultrasonic vibration, the

volume diameter of 10% powder (D_{10}) produced at 650°C calcination is 3.17 μm , showing that 10% of the particles are equal to or less than 3.17 μm and that 90% are greater than 3.17 μm . Other values of D at a variety of conditions are interpreted similarly. D_{50} and mean are totally different. D_{50} divides the powder into two groups containing 50% each, but the mean is the average of all the values. The volume diameters of D_{10} , D_{50} , D_{90} , and mean for nonultrasonic vibration decrease with increasing calcination temperatures. This shows that a group of particles produced at low temperature forms more agglomeration than that at high temperature. For 2 min ultrasonic vibration, D_{50} , D_{90} , and

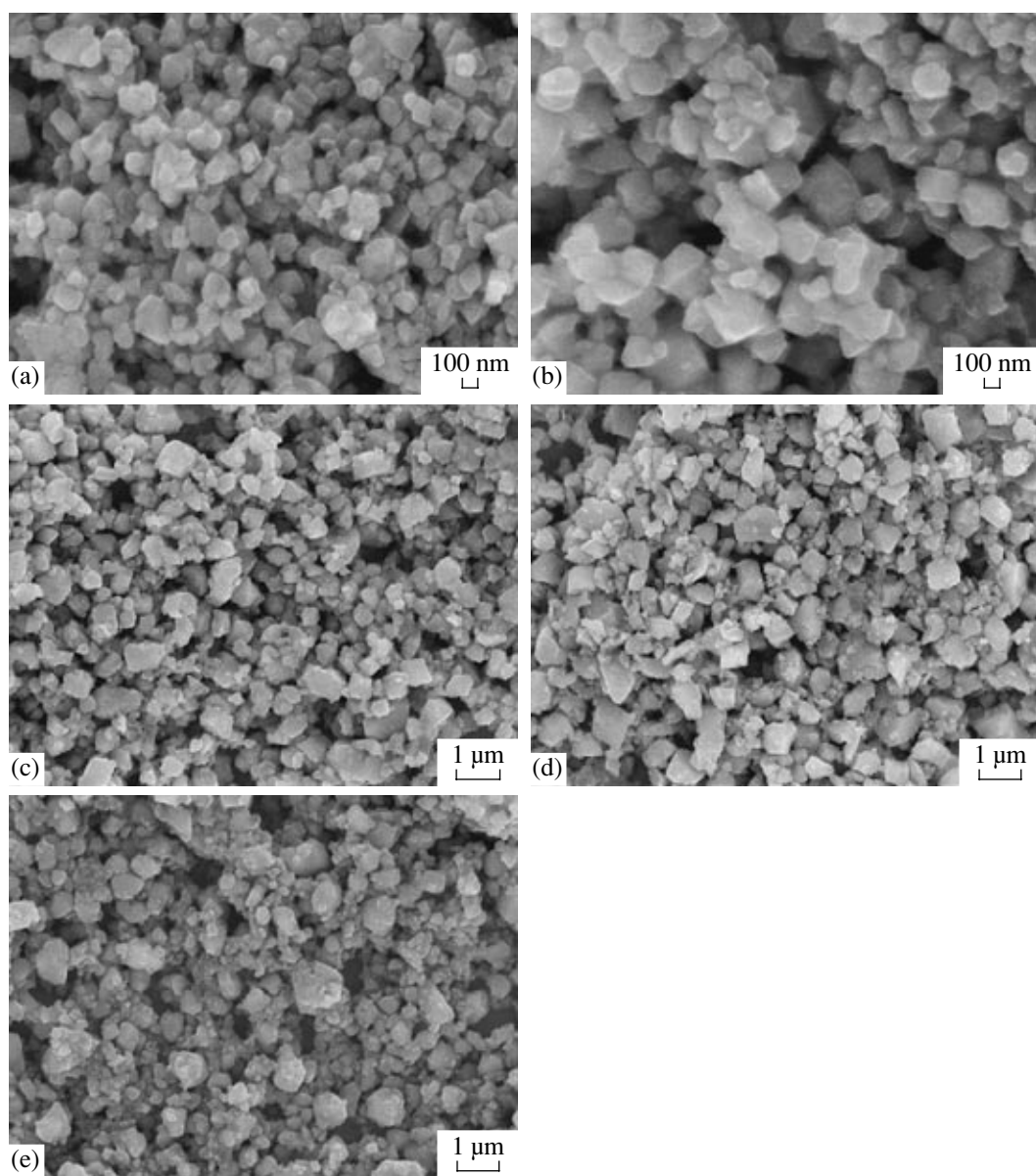


Fig. 9. SEM micrographs of the powder produced at (a) 650°C for 24 h, (b) 700°C for 24 h, (c) 750°C for 24 h, (d) 800°C for 24 h, and (e) 750°C for 40 h.

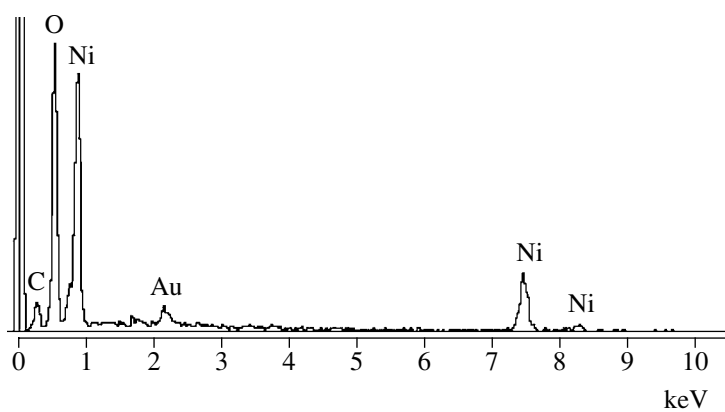


Fig. 10. EDX spectrum of the powder produced at 750°C calcination for 40 h.

Table 2. D10, D50, D90, and mean diameters of the powder for nonultrasonic and ultrasonic vibration

Calcination temperatures, °C	D10, μm	D50, μm	D90, μm	Mean, μm	D10, μm	D50, μm	D90, μm	Mean, μm
	nonultrasonic vibration				ultrasonic vibration (2 min)			
650	3.17	32.59	105.99	45.36	0.94	2.88	10.10	4.39
700	2.07	14.57	73.36	27.94	0.85	3.84	12.03	5.30
750	1.74	12.67	44.93	19.38	1.06	4.52	14.69	6.43
800	1.57	10.80	33.21	15.62	1.31	5.55	17.32	7.68

mean increase with an increase in the calcination temperature, but D10 shows some irregularity. The temperature dependence of the diameter reflects on the distribution shape. Comparing the mean particle diameters for nonultrasonic and ultrasonic vibrations, the former is 2–10 times as large as the latter. When the period of time for ultrasonic vibration was prolonged to 3 min, agglomeration of some tiny particles were detected due to van der Waals attraction. The powder with 750°C calcination for 40 h was analyzed. It was found that the mean for nonultrasonic and 2 min ultrasonic vibrations is 20.81 and 6.55 μm, respectively.

SEM. The powder produced at 650–800°C calcination was analyzed using SEM. The micrographs are shown in Fig. 9. The powder shows different sizes of particles over the range of 0.05–1 μm. The mean diameter increases with increasing calcination temperature, showing that SEM and particle size (with ultrasonic vibration) analyses are in accord. Facets on the particles show that the powder has high crystallinity. Comparing the ranges of particle diameters determined from SEM micrographs and from the particle size analyzer, the former is smaller than the latter due to the agglomeration of tiny particles. SEM micrographs under a high magnification can identify both tiny particles and their agglomerates. The particle size analyzer identifies individual particles as an agglomerate. In addition, the powder produced at 750°C calcination for 40 h is in the range of 0.2–1 μm, which is smaller than that analyzed by the particle size analyzer.

EDX. The powder produced at 750°C calcination for 40 h was analyzed using EDX, and the spectrum is shown in Fig. 10. Li is a light element and cannot be detected. Only Ni and O were detected. This shows the consistency between XRD and EDX analyses. Au and C traces were detected as well. They are from the carbon tape used for sticking the powder onto a copper stub and from sprayed gold on the powder for conductivity improvement.

CONCLUSIONS

$\text{Li}_{1-x}\text{Ni}_{1+x}\text{O}_2$ powder was successfully prepared by a polymerized complex method and subsequent calci-

nation at 650–800°C for 14–48 h. TGA shows that the formation of the oxide seems to begin at 600°C and above. At 650 and 700°C, $\text{Li}_{1-x}\text{Ni}_{1+x}\text{O}_2$ with some impurities was detected. A single phase of $\text{Li}_{1-x}\text{Ni}_{1+x}\text{O}_2$ was detected at 750 and 800°C. The optimum calcination is at 750°C for 40 h. The content of Ni^{3+} and mean oxidation state of Ni at the optimum condition are 60.59 wt % and 2.61, respectively. Ni and O were detected by EDX, which is in accord with the detection of $\text{Li}_{1-x}\text{Ni}_{1+x}\text{O}_2$ by XRD. The particle diameters determined by the particle size analyzer are larger than those shown on the SEM micrographs due to the agglomeration of tiny particles.

ACKNOWLEDGMENTS

This research was supported by the National Research Council of Thailand, Bangkok, and the Faculty of Science, Chiang Mai University, Chiang Mai, Thailand.

REFERENCES

1. Song, M.Y. and Lee, R., Synthesis by Sol–Gel Method and Electrochemical Properties of LiNiO_2 Cathode Material for Lithium Secondary Battery, *J. Power Sources*, 2002, vol. 111, pp. 97–103.
2. Lu, C.H. and Lee, W.C., Novel Emulsion Process for Synthesizing Submicron Lithium Nickel Oxide Powder Used in Lithium Ion Batteries, *Mater. Lett.*, 1999, vol. 40, pp. 103–108.
3. Yamada, S., Fujiwara, M., and Kanda, M., Synthesis and Properties of LiNiO_2 as Cathode Material for Secondary Batteries, *J. Power Sources*, 1995, vol. 54, pp. 209–213.
4. Rao, M.M., Jayalakshmi, M., Schaf, O., *et al.*, Electrochemical Behaviour of Solid Lithium Nickelate (LiNiO_2) in an Aqueous Electrolyte System, *J. Solid State Electrochem.*, 1999, vol. 4, pp. 17–23.
5. Fey, G.T.K., Subramanian, V., and Chen, J.G., Synthesis of Non-stoichiometric Lithium Nickel Cobalt Oxides and Their Structural and Electrochemical Characterization, *Electrochem. Commun.*, 2001, vol. 3, pp. 234–238.
6. Arai, H., Okada, S., Sakurai, Y., and Yamaki, J.I., Thermal Behavior of $\text{Li}_{1-y}\text{NiO}_2$ and the Decomposition

- Mechanism, *Solid State Ionics*, 1998, vol. 109, pp. 295–302.
7. Hwang, B.J., Santhanam, R., and Chen, C.H., Effect of Synthesis Conditions on Electrochemical Properties of $\text{LiNi}_{1-y}\text{Co}_y\text{O}_2$ Cathode for Lithium Rechargeable Batteries, *J. Power Sources*, 2003, vol. 114, pp. 244–252.
 8. Lu, C.H. and Wei-Cheng, L., Reaction Mechanism and Kinetics Analysis of Lithium Nickel Oxide during Solid-State Reaction, *J. Mater. Chem.*, 2000, vol. 10, pp. 1403–1407.
 9. Chang, C.C. and Kumta, P.N., Particulate Sol–Gel Synthesis and Electrochemical Characterization of LiMO_2 ($M = \text{Ni}, \text{Ni}_{0.75}\text{Co}_{0.25}$) Powders, *J. Power Sources*, 1998, vol. 75, pp. 44–55.
 10. Rao, M.M., Liebenow, C., Jayalakshmi, M., *et al.*, High-Temperature Combustion Synthesis and Electrochemical Characterization of LiNiO_2 , LiCoO_2 , and LiMn_2O_4 for Lithium-Ion Secondary Batteries, *J. Solid State Electrochem.*, 2001, vol. 5, pp. 348–354.
 11. Huang, X., Ma, J., Wu, P., *et al.*, Hydrothermal Synthesis of LiCoPO_4 Cathode Materials for Rechargeable Lithium Ion Batteries, *Mater. Lett.*, 2005, vol. 59, pp. 578–582.
 12. Lin, S.P., Fung, K.Z., Hon, Y.M., and Hon, M.H., Crystallization Mechanism of LiNiO_2 Synthesized by Pechini Method, *J. Cryst. Growth*, 2001, vol. 226, pp. 148–157.
 13. Choi, Y.M., Pyun, S.I., Moon, S.I., and Hyung, Y.E., A Study of the Electrochemical Lithium Intercalation Behavior of Porous LiNiO_2 Electrodes Prepared by Solid-State Reaction and Sol–Gel Methods, *J. Power Sources*, 1998, vol. 72, pp. 83–90.
 14. Bianchi, V., Caurant, D., Baffier, N., *et al.*, Synthesis, Structural Characterization, and Magnetic Properties of Quasistoichiometric LiNiO_2 , *Solid State Ionics*, 2001, vol. 140, pp. 1–17.
 15. Burukhin, A., Brylev, O., Hany, P., and Churagulov, B.R., Hydrothermal Synthesis of LiCoO_2 for Lithium Rechargeable Batteries, *Solid State Ionics*, 2002, vol. 151, pp. 259–263.
 16. Tsumura, T., Kishi, S., Konno, H., *et al.*, Structure and Thermal Decomposition of Lithium–Manganese Dicarboxylate Systems, *Thermochim. Acta*, 1996, vol. 278, pp. 135–144.
 17. Lee, Y.S., Sun, Y.K., and Nahm, K.S., Synthesis and Characterization of LiNiO_2 Cathode Material Prepared by an Adipic Acid-Assisted Sol–Gel Method for Lithium Secondary Batteries, *Solid State Ionics*, 1999, vol. 118, pp. 159–168.
 18. *Powder Diffraction File*, Swarthmore: Joint Committee on Powder Diffraction Standards, 19073-3273.
 19. Fey, G.T.K., Shiu, R.F., Subramanian, V., *et al.*, $\text{LiNi}_{0.8}\text{Co}_{0.2}\text{O}_2$ Cathode Materials Synthesized by the Maleic Acid Assisted Sol–Gel Method for Lithium Batteries, *J. Power Sources*, 2002, vol. 103, pp. 265–272.